University of Groningen

Micromechanics of the growth of a craze fibril in glassy polymers

Basu, S; Mahajan, DK; Van der Giessen, E; Mahajan, Dhiraj K.

IMPORTANT NOTE: You are advised to consult the publisher's version (publisher's PDF) if you wish to cite from it. Please check the document version below.

Document Version
Publisher's PDF, also known as Version of record

[Link to publication in University of Groningen/UMCG research database](#)

Micromechanics of the growth of a craze fibril in glassy polymers

Sumit Basu[a,*], Dhiraj K. Mahajan[a], Erik Van der Giessen[b]

[a]*Department of Mechanical Engineering, Indian Institute of Technology, Kanpur 208016, UP, India*
[b]*Materials Science Center, University of Groningen, Nijenborgh 4, 9747 AG Groningen, The Netherlands*

Abstract

The primary objective of this work is to model the growth and eventual failure of a craze fibril in a glassy polymer, starting from a primitive fibril. Experimental investigations have shown that properties like the entanglement density of a polymer play a pivotal role in determining whether macroscopic failure of a polymer occurs through crazing or shear yielding. Failure is seen to be related to the formation of a soft 'active zone' at the craze-bulk interface, through disentanglement. The present work aims at explaining some of the experimental findings about fibril growth and failure in glassy polymers on the basis of a continuum model of a craze with a constitutive model that accounts for yield, network hardening and disentanglement. The results show that this approach is capable of providing explanations for experimentally observed facts such as the propensity to crazing in polymers with low entanglement density and the linearity between the stretch in a fibril and the maximum stretch of a molecular strand in the fibril.
© 2005 Elsevier Ltd. All rights reserved.

Keywords: Amorphous polymers; Crazing; Disentanglement

1. Introduction

A predominant fracture mechanism in polymeric materials is crazing. Crazes are planar crack-like defects, where the two faces of the craze are bridged by thin fibrils. Upon application of stress, crazes widen, leading to stretching of the bridging fibrils until eventual failure. The fibrils render the craze some stress-bearing capabilities until their breakdown leads to the formation of a crack. An understanding of the craze widening and failure processes is, therefore, important to gain insight into the mechanics of fracture in these materials.

It is instructive at this stage to look at successive idealisations of the craze structure as depicted by Estevez et al. [12]. Fig. 1(a) is a schematic of a craze as an interconnected structure of voids and polymer fibrils. Though the load-carrying capacity of the craze stems mainly from the 'primary' fibrils oriented normal to the craze plane, it is now known that the cross-tie fibrils also bear some amount of load (see, Ref. [9]). For our purpose,

however, the cross-tie fibrils are ignored and the craze is idealised as being bridged by a number of cylindrical fibrils, Fig. 1(b). These fibrils again are of two types: primitive fibrils close to the craze tip and much thinner, mature fibrils spanning the rest of the craze. A further abstraction of the craze structure involves 'lumping' the three-dimensional physical picture of Fig. 1(b) into a so-called 'cohesive zone' (or cohesive surface) governed by a constitutive law between the craze opening Δ_n and the normal traction σ_n acting on its faces. This idea, as shown in Fig. 1(c), was used by Estevez et al. [12] in the form of a cohesive zone model for crazing under Mode I, plane strain conditions. The success of such a model depends solely on the ability of the assumed traction-separation law to mimic the actual physical response of a craze to the same normal tractions.

Much of our current understanding of this physical response is born out of detailed experimental investigations into craze growth and failure done by Kramer and co-workers (e.g. Refs. [10,15]). Particularly striking among their findings is the fact that the volume fraction v_f of the mature fibrils remains constant over the length of the craze (i.e. in the x_1-direction in Fig. 1) at all cross-sections along the fibrils (i.e. for all values of x_2), except at the midriff ($x_2 \simeq 0$), where the stretch in the fibril is found to be significantly larger. It follows therefore that, under the

---

* Corresponding author. Tel.: +91 5122597506; fax: +91 5122597408.
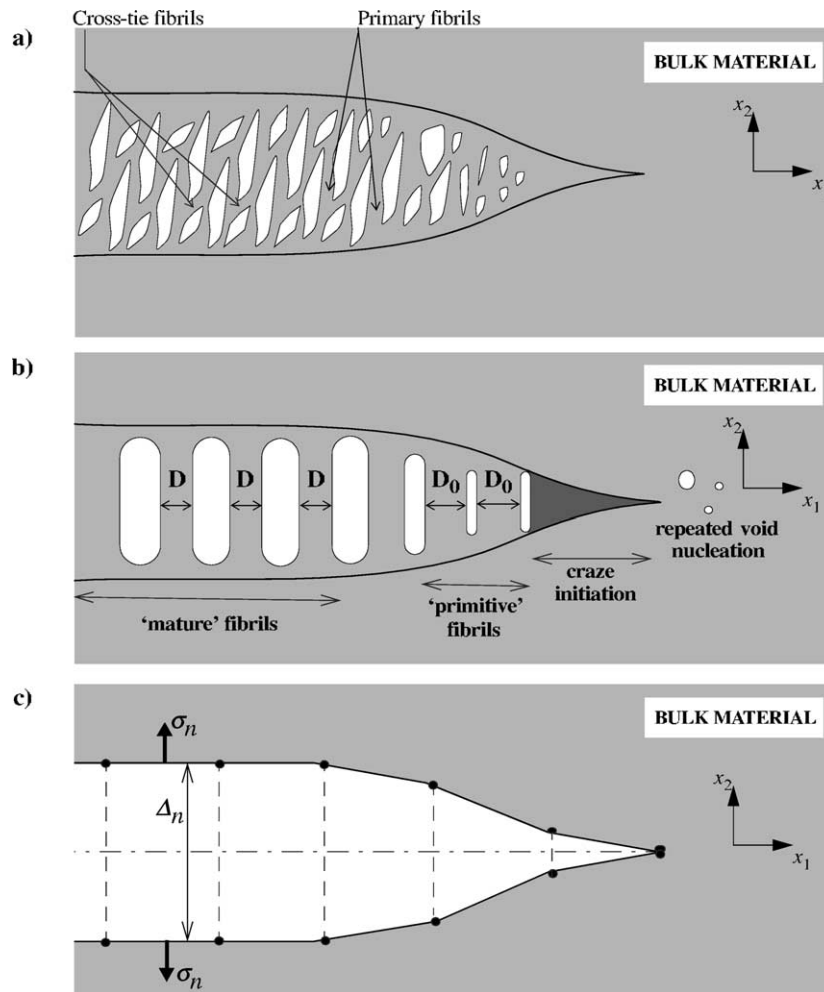 *E-mail address:* sbasu@iitk.ac.in (S. Basu).

Fig. 1. Schematic representation of (a) a real craze, (b) the idealisation of a craze according to Kramer and Berger [15] and (c) as discrete cohesive surfaces.

assumption of incompressibility, the local stretch $\lambda = 1/v_f$ is also a constant. At any point on a fibril, along the x_2 direction, the fibril diameter can be expressed as $D = D_0 \lambda^{-1/2}$ in terms of the diameter D_0 of a primitive fibril and hence, D is a constant as well. The value of λ has been inferred from optical measurements of v_f by Donald and Kramer [11] along a craze fibril (i.e. in the x_2-direction in Fig. 1) and was found to be almost the same all along the length, except at the midriff where it is generally significantly larger. The stretch λ, measured either at the midriff or elsewhere over the fibril length, is in turn found to be directly proportional to the maximum stretch λ_{max} of a molecular strand between entanglements. Moreover, since λ_{max} is an indicator of the entanglement density of the material, these findings suggest that increasing the entanglement density is a viable way of craze suppression. Indeed, it is found that materials with low entanglement density are more prone to crazing than ones with high entanglement density (see, Ref. [14]).

The quantity λ_{max} also appears in constitutive models for elastoviscoplasticity of glassy polymers, which according to Ref. [13] can be idealized as a network of entangled long molecules embedded in the flowing continuum. At large strains, the network stretches considerably, leading to a rather steep hardening regime. The hardening continues till a limit stretch is reached, beyond which the material 'locks' in the sense that it no longer deforms plastically. The material becomes almost rigid after locking and therefore it's stiffness is arbitrarily increased to five times that at zero strain. The mechanical response of the network is governed by two parameters: the density of molecular strands between entanglements, n, and the number of statistical segments N making up each strand. Their product, nN, represents the number of monomers in a unit volume of the material. The maximum stretch that a strand can undergo according to standard non-Gaussian description is then given by $\lambda_{max} = \sqrt{N}$. A continuum model of this type has been used by Tijssens and Van der Giessen [21] to study the widening of a craze, but it did not pick up the remarkable correlation between the fibril stretch and λ_{max} mentioned above.

The objective of this paper is to improve on this and build a more physically realistic continuum description of the widening and failure mechanisms of a craze fibril in a amorphous glassy polymer. With this model in place, we compute the overall response of a craze subject to an

imposed widening. These results are then used to formulate traction-separation laws to be used for cohesive zone models of craze growth and failure in glassy polymers, in the spirit of Estevez et al. [12].

This work can be considered a refinement on similar earlier work by Argon et al. [2] and Boyce et al. [7]. Argon et al. [2] have reported a Finite element analysis on the drawing of peridically arranged craze tufts from a half space using a elastic-rate independent plastic model of polymers. Boyce et al. [7] has analysed the process of cold drawing of a circular polymeric bar using a constitutive response similar to what has been used in the present work. However, the results of this analysis cannot be directly applied to the mechanics of growth of a craze fibril because of two reasons. Firstly, a craze represents an array of fibrils and it is their collective response that a cohesive zone model for crazing should hope to emulate. Secondly, neither Boyce et al. [7] nor Argon et al. [2] have accounted for disentanglement in their continuum models.

2. Continuum modeling of a craze fibril

Depending on the material, craze fibrils have dimensions between a few and tens of nanometers. This raises the question if a continuum model is applicable. The answer to this question can only be given when the predictions of such a model be compared to the results of a molecular length-scale model. A necessary condition for the continuum model to be applicable is that it represents the essential physical phenomena. While we shall be interested mainly in qualitative features here, we envision that the material parameters appearing in the continuum model can, at some point, be fitted to molecular-level properties.

Like in the continuum models of Refs. [15,16], the pulling-in of fibril material from the bulk is described by a model for flow. The already drawn fibrils, represented by the pillars in the cartoon of Fig. 2, cause flow by high shear

stresses in what Kramer and Berger [15] called the 'active zone' connecting adjacent fibrils. The particular model we adopt here is similar to that used by Ref. [21], which is based on formulations by Refs. [8,22], but extended to account for disentanglement inside this active zone. The model is motivated by the following considerations.

Kramer and Berger [15] have suggested that a certain amount of 'geometrically necessary' strand loss accompanies craze growth. Berger [5] attributed this to loss of entangled strands from the polymer network. This loss occurs primarily from the strain-softened boundary between the isotropic polymer bulk and the highly oriented craze fibrils. In fact, Berger and Sauer [6] have demonstrated that the mobility of polymer chains in the craze can be many times higher than a bulk polymer even at temperatures well below the glass transition temperature, making chain pull-out from the network a possibility even at these low temperatures. In addition to the active zone being softer than undistsurbed bulk material, it has been observed by Berger [5] that the failure of a craze almost always starts from this craze-bulk interphase in the form of a pear-shaped void.

Termonia and Smith [19,20] have proposed a Monte-Carlo based lattice model for the deformation of a polymer sample. More recently, Baljon and Robbins [4] have performed molecular simulations on detailed atomistic models of crazes. Both these simulations have underlined the role of chain scission and pull-out (by reptation) of polymer chains on the overall stress–strain response of the craze fibril. But, the constitutive models of Refs. [8,22] consider the entanglement density to remain unchanged during deformation. This needs modification in order that strain-softening due to strand loss can be taken into account, as will be presented in Section 3.

Further, simplifications to the already idealized picture of a widening craze in Fig. 1(b) lead to a unit cell model for the fibril (Section 4). Results for this model are then presented in Section 5, and discussed in the light of experimental facts in Section 6.
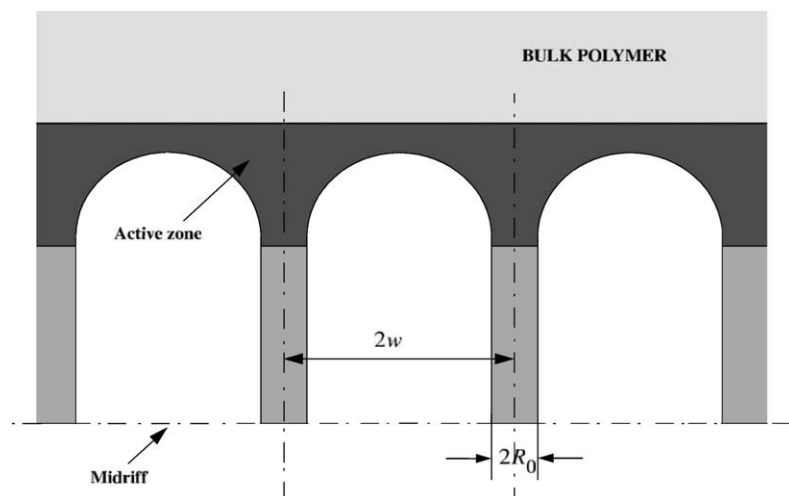

Fig. 2. Schematic showing the geometry of the craze bulk interface.

3. Constitutive law for glassy polymers

The constitutive model was originally proposed by Boyce [8] and later modified by Wu and van der Giessen [22]. The actual form adopted here, as well as the numerical integration scheme used in the calculations have been presented by Wu and van der Giessen [23]. Appropriate modifications to include stress-induced loss of entanglement points are discussed subsequently. The constitutive model starts by assuming that under isothermal conditions the elastic response for small elastic strains can be formulated in terms of the following rate equation for the Cauchy stress tensor $\boldsymbol{\sigma}$:

$$\overset{\triangledown}{\boldsymbol{\sigma}} = \mathcal{L}^{e} : \mathbf{D}^{e} \tag{1}$$

where $\overset{\triangledown}{\boldsymbol{\sigma}}$ is the Jaumann stress rate, $\mathbf{D}^{e}$ is the elastic part of the strain rate tensor $\mathbf{D}$, $\mathbf{D} = \mathbf{D}^{e} + \mathbf{D}^{p}$, and $\mathcal{L}^{e}$ is the tensor of elastic moduli given in the usual way in terms of Young's modulus E and Poisson's ration ν by

$$\mathcal{L}^{e}_{ijkl} = \frac{E}{2(1+\nu)} \left[(\delta_{ik}\delta_{jl} + \delta_{il}\delta_{jk}) + \frac{2\nu}{1-2\nu} \delta_{ij}\delta_{kl} \right] \tag{2}$$

The plastic strain-rate tensor $\mathbf{D}^{p}$ is defined, under the assumption that rate-dependent yield in amorphous polymers is an isotropic process, through

$$\mathbf{D}^{p} = \frac{\dot{\gamma}_{p}}{\sqrt{2}\bar{\tau}} \bar{\boldsymbol{\sigma}}, \quad \bar{\tau} = \sqrt{\frac{1}{2}\bar{\boldsymbol{\sigma}}' : \bar{\boldsymbol{\sigma}}'}, \quad \dot{\gamma}_{p} = \sqrt{\mathbf{D}^{p} : \mathbf{D}^{p}} \tag{3}$$

with $( )'$ denoting the deviatoric part of the driving stress tensor. The driving stress tensor itself is defined as $\bar{\boldsymbol{\sigma}} = \boldsymbol{\sigma} - \mathbf{b}$, where $\mathbf{b}$ is the back stress tensor due to orientation hardening. Viscoplastic flow is described by taking the equivalent plastic shear rate $\dot{\gamma}_{p}$ in (3) be governed by the equivalent shear stress $\bar{\tau}$ according to Argon's [1] expression

$$\dot{\gamma}_{p} = \dot{\gamma}_{0} \exp\left[-\frac{As_{0}}{T}\left\{ 1 - \left(\frac{\bar{\tau}}{s_{y}}\right)^{5/6} \right\} \right] \tag{4}$$

Here, $\dot{\gamma}_{0}$ and A are material parameters and T is the absolute temperature. The quantity $s_{y} = s + \alpha p$ is the pressure (p) dependent athermal shear strength, with α the pressure sensitivity. The strain softening upon yield exhibited by amorphous polymers is taken into account by letting the quantity s evolve according to

$$s = h\left(\frac{1-s}{s_{ss}}\right)\dot{\gamma}_{p} \tag{5}$$

with h the initial softening modulus and s_{ss} the ultimate minimal shear strength [8].

The progressive hardening of a glassy polymer after yield is due to the deformation induced molecular orientation along the plastic stretch direction and is incorporated through the back stress $\mathbf{b}$ in the driving stress $\bar{\tau}$, see Eq. (3). The description of this hardening makes use

of the analogy with the stretching of the cross-linked network in rubbers (cf. Ref. [8]). Neglecting the elastic strains, the constitutive equations for the back stress tensor $\mathbf{b}$ are formulated through a functional description of its principal components b_{α} on the unit principal directions $\mathbf{e}_{\alpha}$ of the left stretch tensor, in terms of the corresponding principal stretches λ_{α}, i.e.

$$\mathbf{b} = \sum_{\alpha} b_{\alpha}(\mathbf{e}_{\alpha} \otimes \mathbf{e}_{\alpha}), \quad b_{\alpha} = b_{\alpha}(\lambda_{\beta})$$

Here, to avoid confusion, principal tensor components and the corresponding eigenvectors are denoted with Greek indices, for which the summation convention is not implied. The constitutive model used here, was proposed by Ref. [22] on the basis of their description of the fully three-dimensional orientation distribution of molecular chains in a non-Gaussian network. They showed that their numerical computations for such a network can be captured very accurately by the following combination of the classical three-chain network description and the eight-chain model due to Arruda and Boyce [3]:

$$b_{\alpha} = (1-\rho)b_{\alpha}^{3-\text{ch}} + \rho b_{\alpha}^{8-\text{ch}} \tag{6}$$

with the weighting factor ρ being determined by the maximum plastic stretch $\bar{\lambda} = \max(\lambda_{1}, \lambda_{2}, \lambda_{3})$ through $\rho = 0.85\bar{\lambda}/\sqrt{N}$. Here, N is the average number of links in a molecular chain between entanglements (or cross-links in a rubber), which determines the limit stretch $\lambda_{\max}$ of a chain as $\lambda_{\max} = \sqrt{N}$. The principal back stress components $b_{\alpha}^{3-\text{ch}}$ and $b_{\alpha}^{8-\text{ch}}$ are given by

$$b_{\alpha}^{3-\text{ch}} = \frac{1}{3}C_{R}\sqrt{N}\lambda_{\alpha}\mathcal{L}^{-1}\left(\frac{\lambda_{\alpha}}{\sqrt{N}}\right) \tag{7}$$

$$b_{\alpha}^{8-\text{ch}} = \frac{1}{3}C_{R}\sqrt{N}\frac{\lambda_{\alpha}^{2}}{\lambda_{c}}\mathcal{L}^{-1}\left(\frac{\lambda_{c}}{\sqrt{N}}\right); \quad \lambda_{c}^{2} = \frac{1}{3}\sum_{\beta=1}^{3}\lambda_{\beta}^{2} \tag{8}$$

where $\mathcal{L}$ is the Langevin function $\mathcal{L}(\beta) = \coth\beta - 1/\beta$. The material constant C_{R} in (7) and (8) governs the initial hardening modulus in shear. When the value of either $\bar{\lambda}$ or λ_{c} approaches $\lambda_{\max}$, the hardening rate increases dramatically, thereby effectively suppressing all further plastic flow, and the network locks. In the calculations, when either λ_{α} or λ_{c} exceeds $0.99\lambda_{\max}$, the network is 'locked' and no further viscoplastic flow is allowed. Fig. 3 shows the typical true stress-true strain response of a glassy polymer in uniaxial tension according to the above model. The stretch at which the material 'locks' is indicated by a dot. Though a qualitative analysis of crazing is being attempted in this work, the material parameters used are representative for polycarbonate (PC) and are given in Table 1.

The entanglement density enters the above constitutive law through the hardening parameters N and C_{R}, which can be expressed as $C_{R} = nkT$ in terms of the density of molecular strands between entanglement points n (k is Boltzmann's constant and T is temperature). Loss of
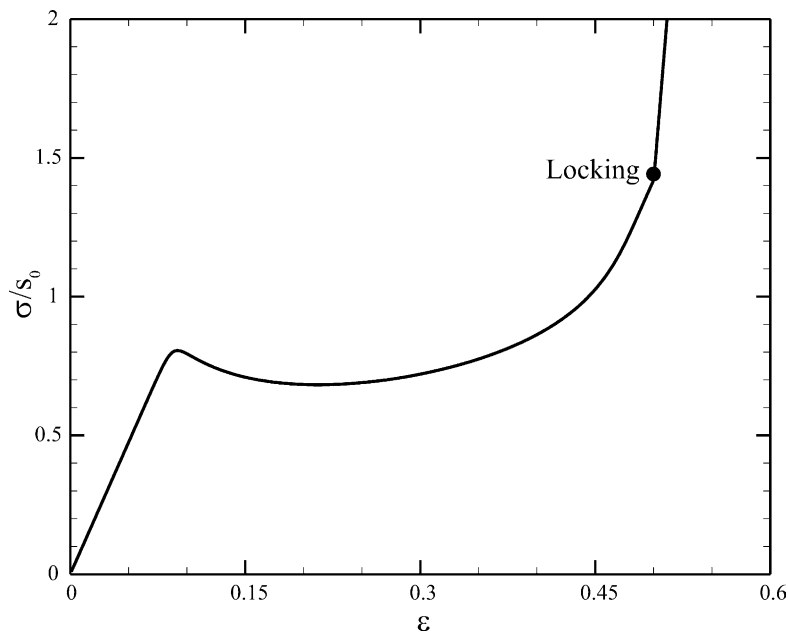
Fig. 3. Uniaxial stress (σ/s_0) vs. strain (ε) response of polycarbonate (PC) in tension. The 'locked' state is shown by a solid dot.

entanglements, and therefore loss of the number of strands, would lead to a decrease of n. The quantity nN remains constant since the molecular weight of the polymer is unchanged. The analyses done in this work will be in the spirit of the experiments of Henkee and Kramer [14] where, to study the effect of strand density on crazing, polystyrene films of a fixed molecular weight were crosslinked to produce various network strand densities by electron irradiation. Also, Termonia and Smith [20] looked at the effect of the entanglement spacing alone on the deformation behaviour of polymers. Strand loss through disentanglement has been modelled by Refs. [19,20] in the framework of a Monte-Carlo simulation of a two-dimensional entangled network of polymer chains. The basic assumption in their model is that slippage of molecular chains through an entanglement point takes place when the forces on two strands of the chain connected to an entanglement point are different. In a time interval $\tau_{th} = 1/\nu_{th}$, where ν_{th} is the frequency of thermal vibrations of an atom, the probability that a particular strand slips through an entanglement point is given by

$$p_0 = \exp\left(-\frac{U_0 - \beta\Delta b_{eq}}{kT}\right) \qquad (9)$$

Hence the number of slip events taking place per second is simply $p_0\nu_{th} = p_0/\tau_{th}$. In the above equation, U_0 is the activation energy, β is the activation volume (i.e. the volume occupied by the segments of the chain which have

to be moved in each slip event) and Δb_{eq} is the difference in network stress between two strands of the same chain connected to a common entanglement point. Termonia and Smith [19,20] suggest that a slip event should be defined as the coordinated movement of one or two statistical segments and hence the activation volume β for such a slip event should be of the order of $(5-10\text{ Å})^3$. The presence of Δb_{eq} in the Eq. (9) expresses the idea that the probability of a slip event is high in a region where there is steep variation of the stress over distances comparable to the length of a strand. Several slip events on the same molecular chain would result in it being drawn out of an entanglement point. If all the chains connected to the same entanglement point are drawn out, the entanglement point would cease to exist. So, disentanglement would in general be more infrequent compared to slippage but it seems reasonable to assume that the probability that a particular entanglement point vanishes in a small time interval τ is still given by the form (9), but with different parameters as will be discussed later. Loss of entanglement points would lead to longer chains and lower strand density n. As n is a measure of and linearly related to the entanglement density, disentanglement can be modelled by assuming that the strand density n evolves with time, t, as

$$\frac{\partial n}{\partial t} = -n\frac{p_0}{\tau} \qquad (10)$$

Table 1
Material parameters used for the glassy polymer represented in Fig. 3, resembling PC at room temperature

E/s_0	ν	s_{ss}/s_0	As_0/T	h/s_0	α	N	C_R/s_0
9.38	0.38	0.79	79.21	5.15	0.08	2.8	0.13

where p_0/τ should now be interpreted as the rate at which entanglement points disappear per unit volume.

Two additional assumptions are made at this stage. Firstly, we will use a stress measure b_{eq} instead of a stress difference Δb_{eq} with the additional restriction that (10) is meaningful when applied only to regions where a high stress gradient is expected to exist. The stress measure that we have chosen to use is the equivalent network back stress defined by $b_{eq} = \sqrt{\frac{1}{2}\mathbf{b}\cdot\mathbf{b}}$, cf. Eq. (3). The spherical symmetry of this measure is motivated by the observation that, in a continuum view, the difference in network stress between two strands is averaged out over the entire network sample that a continuum point represents. The second assumption concerns the choice of the physical parameters in the model. The time interval τ and the activation volume β are larger than for the description of slippage through (9). An indirect way of determining the parameters associated with (10) is to assume that the parameters should be such that the physical response of a continuum undergoing stress-induced disentanglement be similar to the results of the Monte-Carlo simulations of Refs. [19,20] where chain slippage is considered. Their simulations, where disentanglement is a culmination of many slip events, show that the primary effect of chain slippage is loss in the stress carrying capacity of the network. We choose $\tau = 10^{-12}$ s and $U_0 = 80$ kcal/mol and then look at uniaxial stress–strain response of the material for various values of β. The value of the activation energy is similar to the height of the energy barrier for viscous flow of polycarbonate (see, Ref. [17]). Fig. 4 shows that for $\beta = (3000 \text{ Å})^3$ rehardening is completely suppressed and the material behaves like an elastic-perfectly plastic solid immediately after the yield drop. On the other hand, when $\beta = (625 \text{ Å})^3$ the rehardening is not suppressed at all and the material behaves almost exactly like the non-disentangling material shown in Fig. 3. For the PC-like material used in this work, pertinent values of β that could lead to lower rehardening lie between $(625 \text{ Å})^3$ and $(3000 \text{ Å})^3$. The uniaxial response for materials with $\beta =$
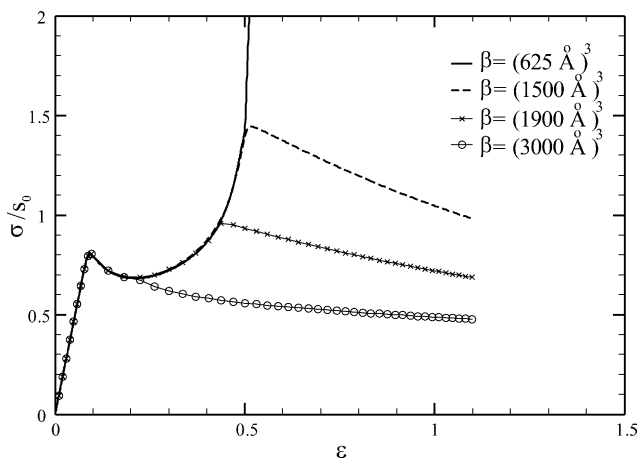

Fig. 4. Uniaxial stress–strain response of a PC-like material in tension, with various values of β representing different disentanglement kinetics.

$(1500 \text{ Å})^3$ and $(1900 \text{ Å})^3$ are also shown in Fig. 4. It is seen that in these cases the material rehardens slightly after the yield drop and then, with progressive disentanglement, softens at higher levels of strain. The value of β chosen for this work is $(3000 \text{ Å})^3$, and so, at a sufficiently high stress level, the material does not reharden at all. By opting for this value of β, we have chosen the fastest possible rate of stress-induced disentanglement. The response of the material for this value of β matches with that obtained by Ref. [19] for a material where chain slippage was permitted (Fig. 2 of their paper).

It should be noted that in the continuum approach adopted in this work, the rate of disentanglement is intimately related to the equivalent back stress b_{eq}. While this is an obvious first step towards understanding the mechanics of growth of a craze fibril, a more detailed (perhaps atomistic) study is needed to uncover all aspects of this process.

4. Unit cell model of a craze

In order to arrive at a numerically tractable model for craze growth, the model presented in Fig. 1(b) is further simplified. Following Ref. [16], we assume that the craze is much longer than it is thick and that the distribution of primitive fibrils can be approximated by a hexagonal array of fibrils, see Fig. 5(a), with a mean spacing $D_0 = 2w$. The behaviour of each fibril can then be represented to good accuracy by an axisymmetric cell containing a single fibril, as shown in Fig. 5(b). Our calculations start from the geometry of a primitive fibril, as defined in Fig. 5(c), where we choose to express all dimensions in terms of the original midriff fibril radius R_0: The half thickness of the craze is $L = 4R_0$ and the half spacing of the fibrils is $w = 2R_0$. With the coordinates as indicated in Fig. 5(c), the displacement boundary conditions for the unit cell are

$$u_1(0, x_2, t) = u_1(w, x_2, t) = 0$$

$$u_2(x_1, 0, t) = 0, \quad u_2(x_1, L, t) = \dot{\Delta} t$$

with $\dot{\Delta}$ the prescribed widening rate of the craze (constant in time, t). All results presented in Section 5 are for $\dot{\Delta}/R_0 = 3.6 \text{ s}^{-1}$.

Note that uniform displacements are prescribed at the top of the cell, $x_2 = L$, in order to represent the large bulk volume on either side of the craze. The resulting stress distribution, $\sigma_{22}(x_1, L)$, will not be uniform, and Σ_{22} denotes its average. As we do not actually model the nucleation of the fibrils, neither the radius R_0 of the initial, primitive fibril nor the state of the material in our initial configuration are known. The value R_0 is somewhat arbitrary, but at the same time it is a key length scale in the model; we will later vary its value to investigate its effect. Also, a primitive fibril in reality will have its molecules oriented to some extent in the
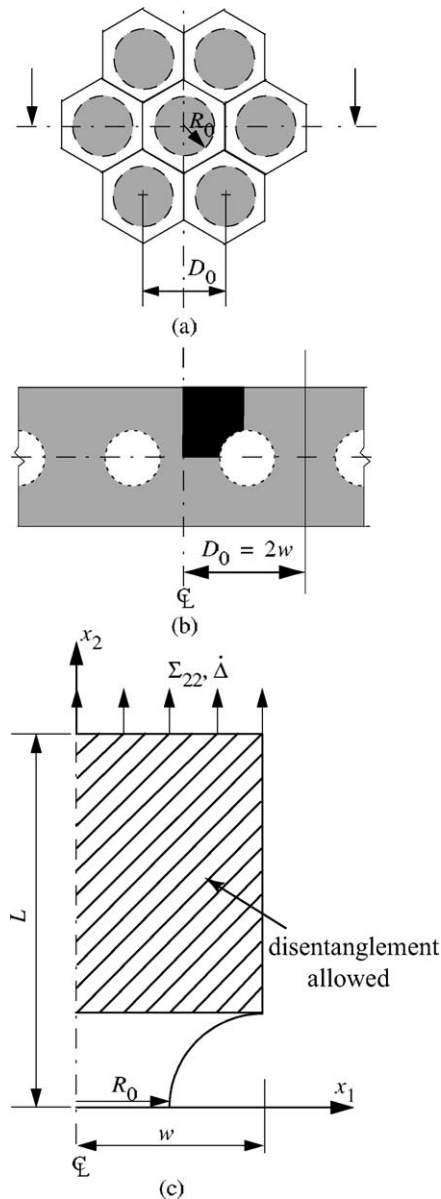
Fig. 5. (a) Idealised distribution of primitive fibrils. (b) A cross-sectional view of the idealised craze structure along the cut in (a). (c) The details of the axisymmetric computational domain representing a single fibril.

direction of stretching, so that the disentanglement is less likely inside the primitive fibril. In our model, we attempt to mimic the effect of this by assuming that the material in the initial configuration of the primitive fibril has randomly oriented molecular strands, but that disentanglement is only potentially possible in the region $x_2 \geq (w - R_0)$, i.e. the hatched region in Fig. 5(c). Hence, it is the region above the dome of the craze where the active zone can form. This is consistent with findings by, e.g. Ref. [5] that this region has a lower entanglement density than the bulk and behaves almost like a non-Newtonian fluid. The analyses are done within the framework of large deformation finite element method, using the constitutive model outlined in Section 3.

Since the objective of this work is to qualitatively assess

the effect of various material parameters on the process of craze growth and failure, no attempt is made to model a particular polymeric material. The basic material properties are those given in Table 1. With $N = 2.8$, this PC-like material has a very high entanglement density, but analyses with other values of N have been performed as well. It should be noted that as nN is held constant, a larger N (larger number of statistical segments between entanglements) implies a smaller n and therefore a lower entanglement density. Entanglement density affects the rehardening response of the material and higher entanglement density leads to stronger rehardening. The values of N used in the analyses to be reported in Sections 5 and 6 are 2.8, 4, 12 and 30. The corresponding values of $C_R = nkT$ at room temperature are 15.8, 11.1, 3.7 and 1.5 MPa, respectively. The values of C_R in turn correspond to initial strand densities $n_0 = n(t = 0)$ ranging from 0.36 to 3.8 nm^{-3}, which are close to strand densities observed in commercial polymers, see Ref. [24]. All other material parameters are kept constant.

5. Results

5.1. Distribution of plastic activity and strand density

Fig. 6 pertains to the material with the highest entanglement density, i.e. $N = 2.8$. Fig. 6(a) shows the distribution of plastic strain rate at two stages of craze widening, namely $\Delta/R_0 = 0.5$ and 1.5. The relative strand density n/n_0 at the same stages of widening are shown in Fig. 6(b). The band of localised plastic strain rate in Fig. 6(a) starts at the midriff ($x_1 = 0$) and travels upwards with increasing widening. The band is accompanied by a region of high stresses ahead of it and leaves behind highly stretched material. Consequently, as the localisation band approaches the craze-bulk interface, the high stresses trigger off the disentanglement process. This is evident even in the first snapshot of Fig. 6(b), for $\Delta/R_0 = 0.5$, where the region with $n/n_0 < 1$ is seen to form just ahead of the shear band. The zone of disentanglement spreads rapidly across the width of the cell and at $\Delta/R_0 = 1.5$, almost the whole craze-bulk interface is bridged by disentangled material ($n/n_0 < 1$).

It should be kept in mind that only the region above the craze dome in the undeformed configuration is allowed to disentangle. Nevertheless, it is seen from Fig. 6(b) that the region with $n/n_0 < 1$ has caved into the stretched fibril. This indicates that material that was above the fibril in the initial configuration has been drawn into the fibril. This observation is similar to that of Kramer and Berger [15] who noted that minute uniformly distributed gold particles in a polymeric sample moved from the craze-bulk interface into the fibrils as they stretched.

The effect of initial entanglement density is demonstrated in Fig. 7 for three stages of widening, $\Delta/R_0 = 0.5$, 1.5 and 5. Evidently, a fibril in a material with a higher value of
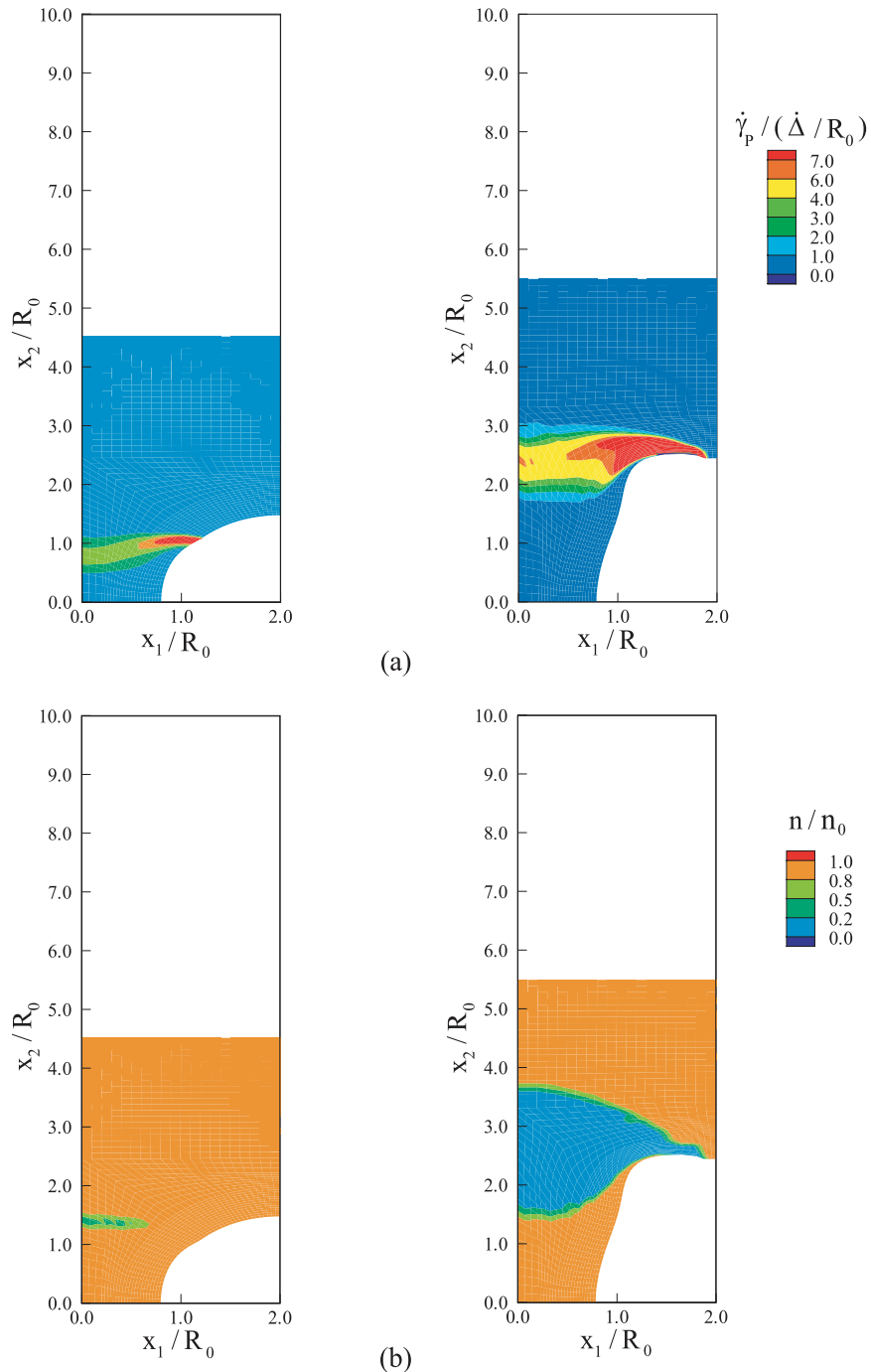
Fig. 6. Contours of (a) plastic strain rate and (b) relative strand density at $\Delta/R_0 = 0.5$ and 1.5 for a polymer with high entanglement density ($N = 2.8$).

N can sustain much higher levels of stretch than a material with low N. For a higher value of N, the band of localised shearing rate moves up slowly relative to the fibril and so the widening Δ/R_0 at which large scale disentanglement sets in is larger. It is seen from Fig. 7(b) that at a widening of $\Delta/R_0 = 1.5$ the disentangled region is much smaller compared to the material with $N = 2.8$, cf. Fig. 6(b). At a much larger widening of $\Delta/R_0 = 5$, however, the whole of the craze-bulk interface has finally been bridged, and a very long and slender fibril has been formed. Henkee and Kramer

[14] have observed that polymers with low entanglement densities are more prone to crazing than materials with higher entanglement densities. This is consistent with the results reported above, where, while keeping nN constant, the results in Fig. 7 are for a lower entanglement density than in Fig. 6. A fibril in a material with low entanglement density (like the one in Fig. 7) can be stretched much more before large scale disentanglement occurs at the craze-bulk interface. Longer fibrils imply wider and, hence, more prominently visible crazes.
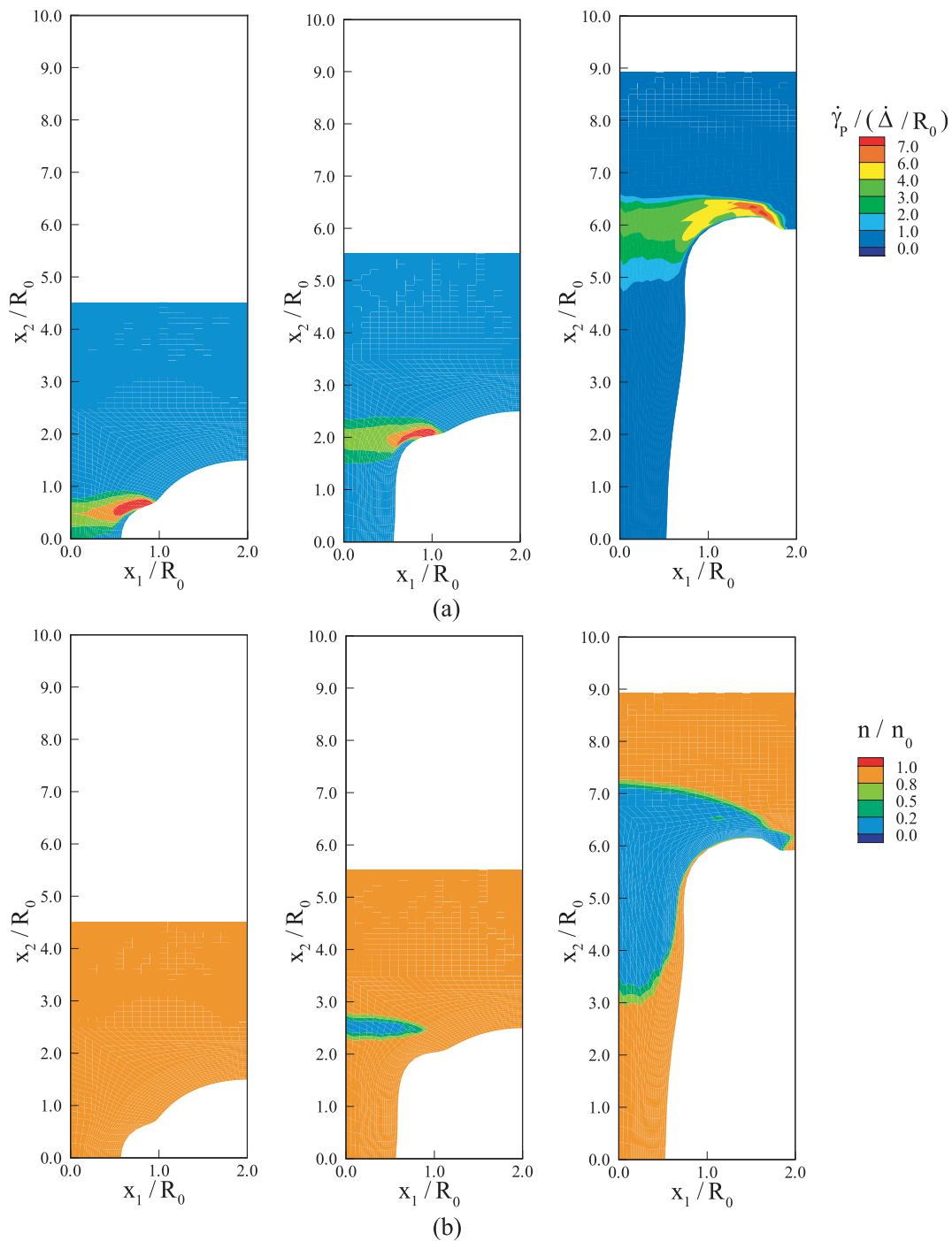
Fig. 7. Contours of (a) plastic strain rate and (b) relative strand density at $\Delta/R_0 = 0.5$, 1.5 and 5.0 for a polymer with low entanglement density ($N = 12.0$).

5.2. Overall widening response

The overall stress-widening responses, i.e Σ_{22}/s_0 as a function of Δ/R_0, for various values of N are presented in Fig. 8. The overall response for the case with $N = 2.8$ shows considerable hardening at $\Delta/R_0 = 0.5$, when disentanglement at the craze-bulk interface has already been triggered. At $\Delta/R_0 = 1.5$, when the whole of the craze-bulk interface has been bridged by disentangled material, the overall response actually begins to drop with increasing stretch. The same overall characteristics are seen for the materials with $N = 4$ and 12, but the hardening is seen to be lower and to set in at higher levels of widening Δ/R_0. For the material with $N = 4$, the stretch at which the stress starts to drop is $\Delta/R_0 = 1.7$ and for the material with $N = 12$, this is $\Delta/R_0 = 4.7$. As for $N = 2.8$, the drop in the overall stress corresponds to large-scale disentanglement at the craze-bulk interface and indicates that the whole of the interface has been bridged by
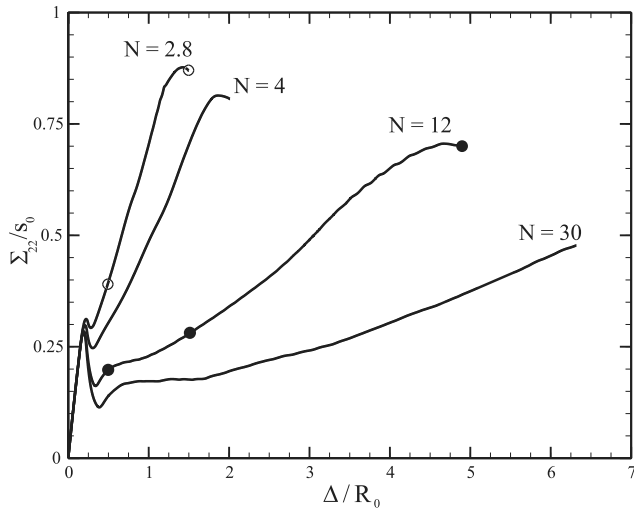
Fig. 8. Overall stress-widening response of the fibril with different values of N. Analyses pertain to an initial configuration with $R_0 = 0.5w$. Open circles indicate the deformation stages in Fig. 6 while filled circles indicate those in Fig. 7.

Fig. 9. Overall stress-widening response of the fibril with different values of N. Analyses pertain to an initial configuration with $R_0 = 0.75w$.

disentangled material. The situation is somewhat different for the material with $N = 30$. In view of the corresponding very low initial entanglement density, the material has a much lower rehardening response and as a result, the stress carrying capacity of the fibril is considerably lower than for the other materials shown in Fig. 8. Such low stress levels at the craze-bulk interface do not lead to any significant disentanglement at the craze-bulk interface and the overall stress rises slowly but monotonically with imposed widening. At such large values of N, the widening required to cause large scale disentanglement would be enormously large and remeshing at the midriff would be necessary in order to continue the calculations to those high levels of widening. This is not attempted in this work.

Rottler and Robbins [18] and Baljon and Robbins [4] have carried out molecular dynamics simulations of craze growth. They assumed a coarse-grained bead-spring model of the polymer and studied flexible as well as semi-flexible polymer chains having varying (but low) entanglement densities. For chains with larger molecular weights, the overall response obtained by Ref. [18] is qualitatively quite similar to that in Fig. 8. They obtain a region with almost constant stress before the crazes start to harden, quite akin what is seen for the case with $N = 30$.

The craze widening stress for a particular value of N depends on the initial fibril diameter. In order to assess the effect of this, we have repeated the calculations for the same N-values but with a thicker primitive fibril: $R_0 = 0.75w$. The overall response of these four materials, as shown in Fig. 9, reveals that the primary effect of increasing the initial fibril radius is, as expected, to increase the craze widening stress. The yield drop in the overall stress commences at a lower value of Δ/R_0 than for the thinner initial fibril.

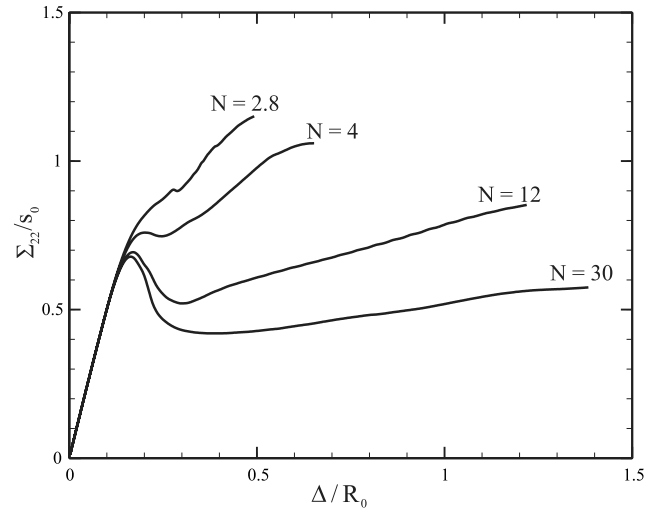However, the stress drop itself is lower for larger R_0. For

the material with $N = 2.8$, the yield drop is almost imperceptible when $R_0 = 0.75w$.

5.3. Stress distributions inside the fibril

In this subsection, we focus on the distribution of normal stress at the midriff A–A′ and above the dome of the craze, B–B′ as defined in the inset of Fig. 10. Both stresses are plotted against the undeformed coordinates x_1/R_0 and x_2/R_0, respectively. Fig. 10(a) shows the normal stress σ_{22} at the midriff for the material with $N = 2.8$ at two stages of widening $\Delta/R_0 = 0.5$ and 1.5, which correspond to the stages in Fig. 6. It is seen that close to the free surface, a thin region of very high stress develops at the midriff. This represents the material with highly stretched molecular chains that have locked. Towards the center line of the fibril, the stresses drop considerably and stay almost constant.

The normal stress σ_{11} along B–B′, i.e. in the dome between two neighbouring fibrils, are shown in Fig. 10(b). At $\Delta/R_0 = 0.5$, the shear bands have not reached the craze-bulk interface and so the stresses on B–B have not been able to rise much. However, as the shear bands arrive at the interface between the craze and the bulk, not only do the stresses rise considerably, but also disentanglement is triggered. As a consequence, the stress levels at $\Delta/R_0 = 1.5$ are much higher except close to the top of the dome due to the disentangled zone. Hence, at $x_2/R_0 \simeq 1.4$, the stress reaches a peak of $\sigma_{11}/s_0 \simeq 0.91$ and then drops to around $\sigma_{11}/s_0 = 0.5$ at $x_2/R_0 = 1$. The region $1 \leq x_2/R_0 \leq 1.4$ roughly gives a measure of the height of the active zone above the craze dome. Qualitatively similar stress distributions were found in materials with higher values of N. These results are significant because it has been postulated by, e.g. Ref. [15], that stresses along B–B′ may cause chains to stretch and break or to get pulled out, which in turn might be a mechanism by which the tip of the dome moves upwards.
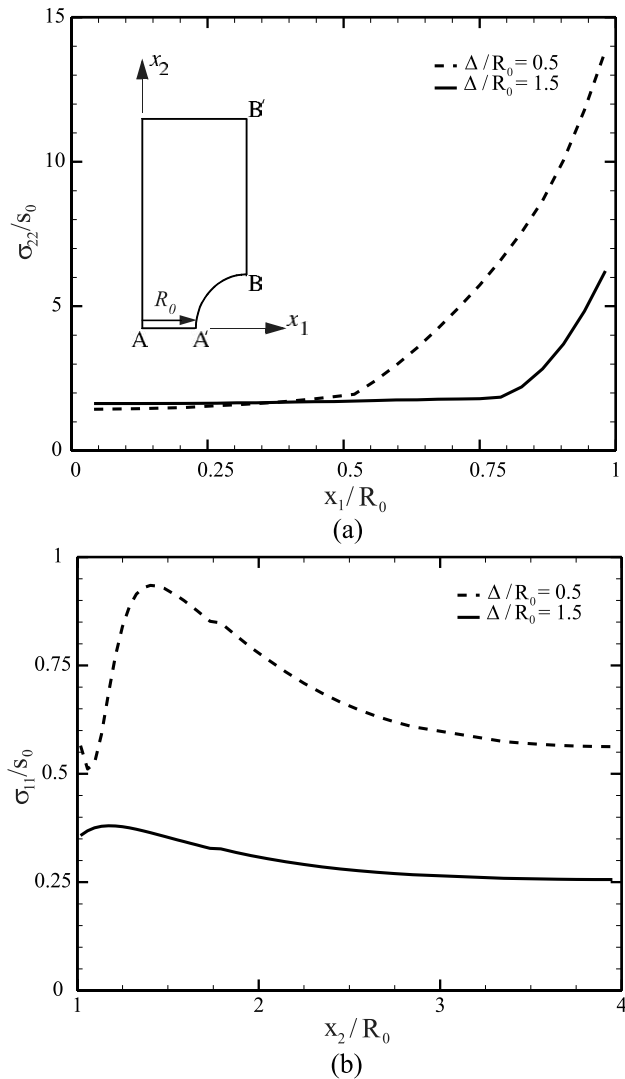
Fig. 10. Variation of (a) the normal stress σ_{22} with x_1 along the midriff A–A$'$ and (b) the normal stress σ_{11} with x_2 along B–B$'$ for $N=2.8$.

However, in view of the rather low stresses along B–B$'$, this seems unlikely.

6. Discussion

The objective of this work, as mentioned in Section 1, is to explain some of the key experimental observations regarding crazing using a relatively simple continuum model. In order to be able to relate to experimental findings, the effect of the rather unrealistic initial state on the subsequent deformation has to be carefully assessed. In other words, it needs to be established that starting from an isotropic cylindrical unit cell containing an initial fibril of R_0 (a configuration which may never occur in reality in a glassy polymer) it is possible to end up with a deformed configuration that resembles a mature craze fibril. A possible definition of a mature fibril can be formulated on

the basis of Ref. [15] experimental observation that the volume fraction v_f at any point along the mature fibril in the longitudinal (x_2) direction remains almost constant as the craze widens. According to this observation, the quantity $(w/R(x_2))^2$, where $R(x_2)$ is the radius of the fibril at x_2, should remain independent of x_2 (the fibril half-spacing w appears here only for dimensional reasons). A special case is the midriff $x_2=0$ with radius R_{mid}. To verify whether $(w/R_{mid})^2$ remains constant, Fig. 11 shows the evolution of the midriff radius R_{mid}/R_0 with craze width Δ/R_0 for various values of N. Initially, R_{mid} decreases with Δ because of elastoplastic contraction of the primitive fibril, but from around $\Delta/R_0 = 0.5$, the rate of decrease of the radius slows down considerably. This appears as the rather sharp 'knee' in all curves in Fig. 11. This is due to the fact that a layer of highly stretched 'locked' material forms at the free surface around this value of the width. Even though the thickness of the 'locked' shell varies with the initial entanglement density, it makes the fibril very stiff and hence resistant to further lateral contraction. Thereafter, the radius at the midriff remains almost constant. This constant value of the radius, however, is smaller for lower entanglement density or increasing value of N.

The fact that the radius becomes constant at a sufficiently large craze width is intimately connected to the disentanglement at the craze-bulk interface. This is illustrated for $N=2.8$ in Fig. 12, by comparing the previous results with midriff evolution when disentanglement is suppressed; in that case, the radius at the midriff does not attain constancy but continues to decrease. However, the 'knee' in the evolution of the radius occurs at the same craze width for both cases. Hence, the knee is a result of the locking of molecular chains while the attainment of constancy is related to the formation of the softer, disentangled active
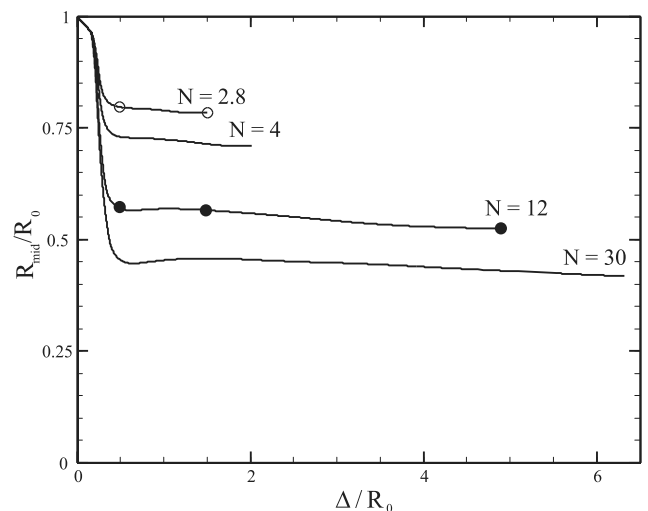

Fig. 11. The evolution of the midriff radius $R_{mid}=R(x_2=0)$ with Δ/R_0 for various values of N. The initial fibril radius is $R_0=0.5w$. The symbols for $N=2.8$ and $N=12$ indicate the stages depicted in Figs. 6 and 7, respectively.
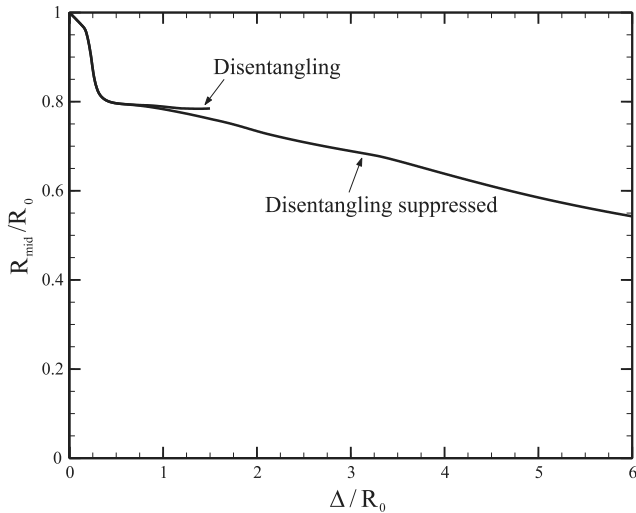
Fig. 12. Effect of disentanglement on the evolution of the midriff radius R_{mid} for a polymer with $N = 2.8$.

region at the craze-bulk interface which effectively shields the rest of the fibril from further deformation.

The craze width at which the 'knee' develops in Fig. 11 can be considered to be the point at which the unit cell starts behaving like a mature craze fibril. In the analyses with $R_0 = 0.75w$, shown in Fig. 13, the 'knee' in the R_{mid}–Δ plots is less sharp than for the cases with $R_0 = 0.5w$, Fig. 11. When the attainment of a constant value of R_{mid} is taken as the condition for a fibril to be 'mature', then (except for the case with $N = 30$) significant hardening takes place (Fig. 8), even in a mature fibril. For $R_0 = 0.75w$, the fibril with the highest entanglement density, (i.e. the one with $N = 2.8$), behaves in a rather brittle manner in the sense that it fails almost as soon as it attains maturation.

Assuming plastic incompressibility of the fibril material, the volume fraction v_f at any cross-section x_2 can be related to the average stretch λ at that cross-section through $\lambda = 1/v_f$.
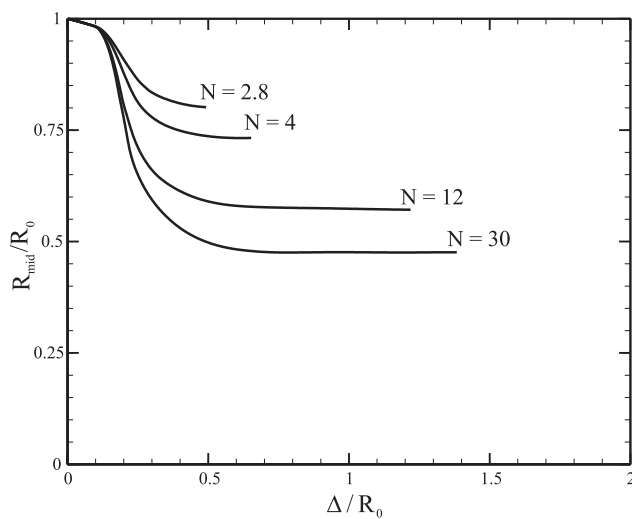
Using this, the reciprocal of the volume fraction can be written as

$$\lambda(x_2) = \left(\frac{w}{R(x_2)} \right)^2 \qquad (11)$$

and gives a measure of the average stretch over the radius at x_2. The variation of λ as a function of x_2/R_0 is shown in Fig. 14. The largest value of λ is found at the midriff ($x_2 = 0$) and it decreases as we move towards the craze-bulk interface. This is in agreement with experimental results presented by Donald and Kramer [10], in particular their Fig. 2. However, in their experimental results, the stretch shows a spike at the midriff and drops rapidly as one moves towards the craze-bulk interface. The gradual drop in the values of stretch seen in Fig. 14 is probably an artifact of the idealised fibril structure adopted in this work (Fig. 1). In Fig. 15, we plot the value of $\lambda(x_2 = 0)$ based on the minimum values of $R_{mid} = R(x_2 = 0)$ (Fig. 11) against $\lambda_{max} = \sqrt{N}$ for $R_0 = 0.5w$. The solid line is a linear fit to the computed points for $R_0 = 0.5w$, and shows that λ scales almost linearly with λ_{max}. The direct proportionality between λ and λ_{max} has been observed experimentally by Kramer and Berger [15] and co-workers. In this work, we have been able to derive it starting from a constitutive description of the polymer and a simple model of a craze fibril. It should be noted, however, that the slope of the line in Fig. 15 is larger than unity, while Kramer and Berger [15] observe that $\lambda \simeq \lambda_{max}$. The slope is a consequence of the initial volume fraction in the unit cell and hence of R_0. To prove this contention, Fig. 15 also shows the results for $R_0 = 0.75w$ and the same values of N (dashed line), which has a slope much closer to unity. We have already argued that our model requires specification of R_0 because we neglect the craze initiation process. In reality, the diameter of the primitive fibril at the start of the drawing process as modelled here is a consequence of the precise

Fig. 13. The evolution of the midriff radius R_{mid}/R_0 with Δ/R_0 for various values of N. The initial fibril radius is $R_0 = 0.75w$.
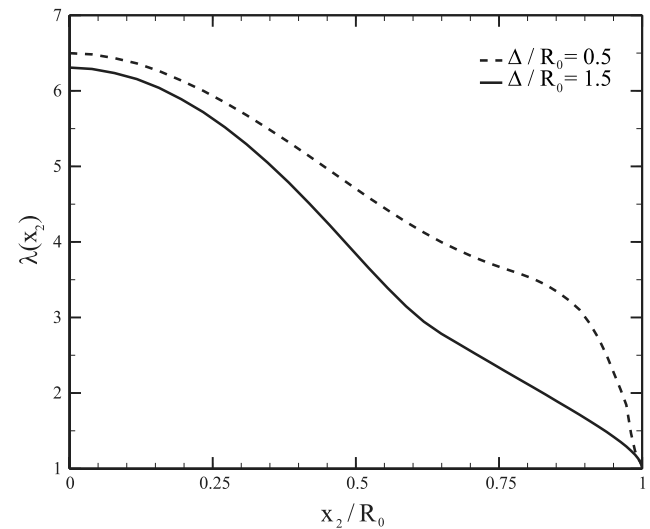

Fig. 14. The average stretch $\lambda(x_2)$, defined by (11), along the fibril at two stages of widening, for a polymer with $N = 2.8$.
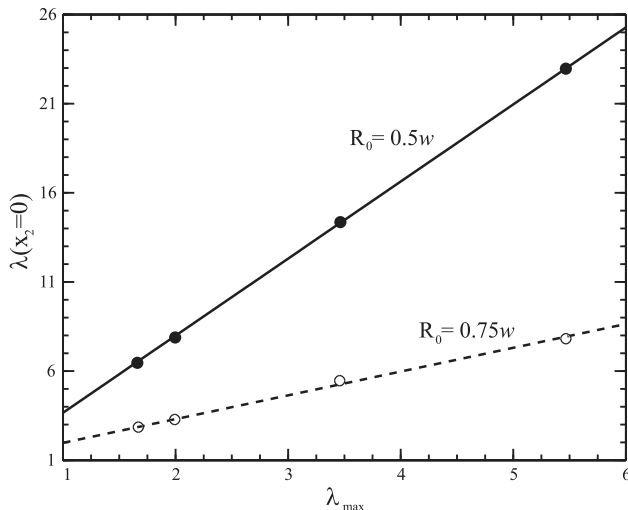
Fig. 15. Average stretch λ, according to (11), at the fibril's midriff versus the material limit stretch $\lambda_{max}(=\sqrt{N})$ for initial configurations with $R_0 = 0.5w$ and $R_0 = 0.75w$.

initiation process; circumstantial evidence from the results found here, suggests that this diameter is probably quite close to the mean fibril spacing.

In addition to providing insight into the craze widening process itself, the computations reported here can help the development of traction-separation laws to be used in cohesive zone models for crazing in a glassy polymer. Thus, the cohesive zone traction-separation relation can be derived from the overall response computed from the present model, e.g. as shown in Figs. 8 and 9. As the present results were not available at the time, Estevez et al. [12] have adopted a phenomenological formulation in which the craze widened by a rate-dependent, non-hardening plastic deformation process, much like the bulk material, until a critical opening Δ_{crit} was reached. While the question of a suitable craze initiation criterion still remains open, the present work offers refinement in two aspects. Firstly, it is seen from Fig. 8 that beyond $\Delta/R_0 = 0.5$, the overall stress Σ_{22} is increasing with widening for all materials considered: the fibrils harden with the hardening being dependent on N. This means that even though the radius at the midriff has already become constant due to the effect of disentanglement (Fig. 11), the associated softening does not affect the overall response until much larger widening. Secondly, the value at which the craze fails, Δ_{crit}, in the cohesive surface law can be obtained from the present computations by identifying Δ_{crit} with the width at which the overall stress starts to decrease, when the craze-bulk interface is bridged by disentangled material. As seen in Fig. 16, which pertains to the case with $R_0 = 0.5w$, Δ_{crit} as well as the corresponding overall peak stress Σ_{22} depend on the strand density n.

The fact that Δ_{crit} decreases with n is consistent with the experimental observation that polymers with low entanglement density are more prone to crazing than the ones with high entanglement density (see also discussion pertaining to

Figs. 6 and 7 in the previous section). The almost linear relation between the craze failure stress and entanglement density is consistent with experimental observations of Ref. [24]. The analyses in Fig. 9 and the additional results in Fig. 13 with a larger initial fibril radius R_0 further underline the fact that higher the entanglement density, more brittle the craze should be. In other words, a highly entangled polymer would fail quickly after attaining maturation. On the other hand a lightly entangled polymer would give rise to long fibrils that expend much energy in craze widening before failing completely. This, however, does not mean that polymers with high entanglement density are tougher than ones with low entanglement density. Toughness is determined by the energy required to make a crack propagate and this is not only controlled by the energy for crazing but also by the energy dissipated by shear yielding around the moving crack tip. This is a different problem than the one studied here, and can be addressed for instance with a cohesive zone representation of crazing, as done by Estevez et al. [12]. The only thing we can deduce from the present work is that if crazing was the only mechanism involved during failure, low entanglement density polymers would consume more energy to fail. This is actually observed by Henkee and Kramer [14] who used a polymer with a fixed molecular weight but varied the crosslink density.

It should be noted finally that Δ_{crit} will depend to some extent on the disentanglement kinetics, particularly the value of β. However, in this qualitative study the parameters U_0 and β were kept constant. More in general, they should be considered as 'fitting parameters', with their values determined by comparison with experimental results or obtained from atomistic simulations.

A further point merits mentioning at this stage. As already elaborated, the role of b_{eq} in causing disentanglement is a simple way of dealing with the complicated issue of stress-induced disentanglement, which at the molecular level requires reptative motion of chains through the entanglement points. While this is, to the best of our knowledge, the first work that is able to reproduce many of the experimental findings of Kramer and co-workers through a continuum model, some issues need further investigation. Kramer and Berger [15] postulate that the mechanism of craze growth is through the process of disentanglement occurring ahead of the dome of the craze, i.e. $X_2 > R_0$. However, according to our model disentanglement starts at the centerline, i.e. in between the craze stems where b_{eq} attains high values earlier, and then propagates towards the craze dome. Resolution of this issue requires a simulation that includes the nucleation process, which is a challenge at this stage.

7. Conclusions

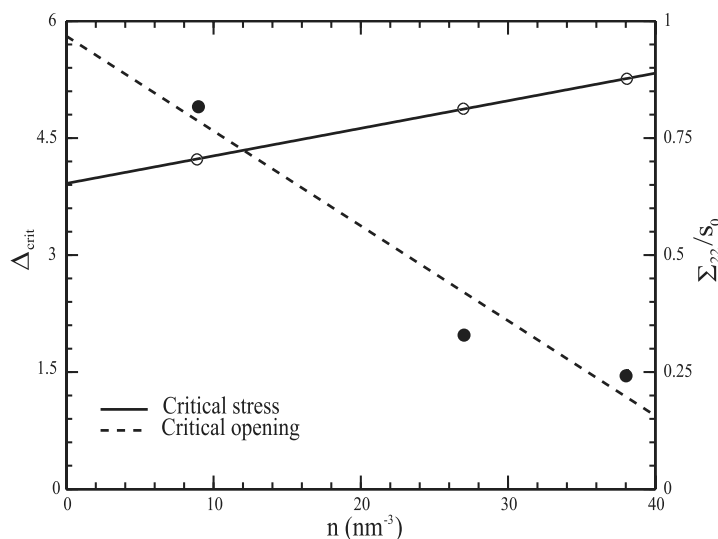A simplified axisymmetric model of a craze fibril has

Fig. 16. The craze width and stress at failure as a function of the initial strand density for various polymers, for the case $R_0 = 0.5w$.

been used to numerically study the process of craze widening leading to the formation of a mature fibril. The material model uses a continuum theory for rate-dependent yield, with softening and subsequent rehardening, supplemented with a simple model for stress-induced disentanglement. Thus, the model provides a refinement of the theories of Kramer and Berger [9,15]. With physically reasonable parameter values, it predicts the following, experimentally known characteristics of crazing:

- Due to disentanglement, the material near the craze-bulk interface softens, thus forming the so-called active zone above a fibril.
- In the course of fibril elongation, material from the bulk is drawn into the craze.
- Polymers with lower entanglement density give rise to longer and more slender fibrils. Consequently, polymers with lower entanglement density have higher values of critical opening at failure but need lower levels of overall stress. A low entanglement density polymer absorbs more energy in the crazing process than a highly entangled one.
- Disentanglement at the craze-bulk interface causes the fibril diameter to reach a constant value.
- The average fibril stretch λ at the midriff cross-section scales linearly with the maximum stretch between two entanglements, λ_{max}.

Quantitative comparison with experimental results awaits the experimental determination of the parameters in the model.

References

[1] Argon AS. A theory for the low-temperature plastic deformation of glassy polymers. Philos Mag 1973;28:839–65.

[2] Argon AS, Cohen RE, Gebizlioglu OS, Brown HR, Kramer EJ. A new mechanism of toughening glassy polymers. Part 2. Theoretical approach. Macromolecules 1990;23:3975–82.

[3] Arruda EM, Boyce MC. A three-dimensional constitutive model for large stretch behaviour of rubber elastic materials. J Mech Phys Solids 1993;41:389–412.

[4] Baljon ARC, Robbins MO. Simulations of crazing in polymer glasses: Effect of chain length and surface tension. Macromolecules 2003;34: 4200–9.

[5] Berger LL. On the mechanism of craze fibril breakdown in glassy polymers. Macromolecules 1990;23:2926–34.

[6] Berger LL, Sauer BB. Enhanced segmental mobility at polymer surfaces: Thermally simulated current studies of crazed films. Macromolecules 1991;24:2096–9.

[7] Boyce M, Montagut EL, Argon AS. The effects of thermomechanical coupling on the cold drawing process of glassy polymers. Polym Eng Sci 1992;32:1073–85.

[8] Boyce M, Parks DM, Argon AS. Large inelastic deformation of glassy polymers. Part 1. Rate dependent constitutive model. Mech Mater 1988;7:15–33.

[9] Brown HR. A molecular interpretation of the toughness of glassy polymers. Macromolecules 1991;24:2752–6.

[10] Donald AM, Kramer EJ. The competition between shear deformation and crazing in glassy polymers. J Mater Sci 1982;17:1871–9.

[11] Donald AM, Kramer EJ. The entanglement network and craze micromechanics in glassy polymers. J Polym Sci, Polym Phys 1982; 20:1129–41.

[12] Estevez R, Tijssens MGA, Van der Giessen E. Modeling of the competition between shear yielding and crazing in glassy polymers. J Mech Phys Solids 2000;48:2585–617.

[13] Haward RN, Thackray G. The use of a mathematical model to describe isothermal stress–strain curves in glassy thermoplastics. Proc R Soc London, Ser A 1968;302:453–72.

[14] Henkee CS, Kramer EJ. Crazing and shear deformation in crosslinked polystyrene. J Polym Sci, Polym Phys 1984;22:721–37.

[15] Kramer HH, Berger LL. Fundamental processes of craze growth and fracture. Adv Polym Sci 1990;91/92:1–68.

[16] Leonov AI, Brown HR. A model for fibril deformation in crazes. J Polym Sci, Polym Phys 1991;29:197–209.

[17] McCrum NG, Buckley CP, Bucknall CB. Principles of polymer engineering. New York: Oxford University Press; 1997.

[18] Rottler J, Robbins MO. Growth, microstructure and failure of crazes in glassy polymers. Phys Rev E 2003;68:011801.

[19] Termonia Y, Smith P. Kinetic model for tensile deformation of polymers. Part 1. Effect of molecular weight. Macromolecules 1987; 20:835–8.

[20] Termonia Y, Smith P. Kinetic model for tensile deformation of polymers. Part 2. Effect of entanglement spacing. Macromolecules 1987;20:835–8.

[21] Tijssens MGA, Van der Giessen E. A possible mechanism for cross-tie fibril generation in crazing of amorphous polymers. Polymer 2002; 43:831–8.

[22] Wu PD, Van der Giessen E. On improved network models for rubber elasticity and their applications to orientation hardening in glassy polymers. J Mech Phys Solids 1993;41:427–56.

[23] Wu PD, van der Giessen E. Computational aspects of localised deformations in amorphous glassy polymers. Eur J Mech, A/Solids 1996;15:799–823.

[24] Yamamoto T, Furukawa H. Relationship between molecular structure and deformation-fracture mechanism of amorphous polymers. Part 2. Crazing stresses. Polymer 1995;36:2393–6.